JOURNAL OF SYNCHROTRON RADIATION

ISSN 1600-5775

Received 11 February 2015
Accepted 19 April 2015

Edited by P. A. Pianetta, SLAC National Accelerator Laboratory, USA

† Deceased.

Keywords: X-ray microscopy; Zernike phase contrast; phase retrieval; phase ring.

Quantitative phase retrieval in X-ray Zernike phase contrast microscopy

Heng Chen,[a,b] Zhili Wang,[b]* Kun Gao,[b] Qiyue Hou,[c] Dajiang Wang[b] and Ziyu Wu[b,d]†

[a]Department of Physics, University of Science and Technology of China, Hefei, Anhui 230026, People's Republic of China, [b]National Synchrotron Radiation Laboratory, University of Science and Technology of China, Hefei, Anhui 230029, People's Republic of China, [c]Institute of Fluid Physics, China Academy of Engineering Physics, Mianyang, Sichuan 621900, People's Republic of China, and [d]Beijing Synchrotron Radiation Facility, Institute of High Energy Physics, Chinese Academy of Sciences, Beijing 100049, People's Republic of China.
*Correspondence e-mail: wangnsrl@ustc.edu.cn

In recent years, increasing attention has been devoted to X-ray phase contrast imaging, since it can provide high-contrast images by using phase variations. Among the different existing techniques, Zernike phase contrast microscopy is one of the most popular phase-sensitive techniques for investigating the fine structure of the sample at high spatial resolution. In X-ray Zernike phase contrast microscopy, the image contrast is indeed a mixture of absorption and phase contrast. Therefore, this technique just provides qualitative information on the object, which makes the interpretation of the image difficult. In this contribution, an approach is proposed for quantitative phase retrieval in X-ray Zernike phase contrast microscopy. By shifting the phase of the direct light by $\pi/2$ and $3\pi/2$, two images of the same object are measured successively. The phase information of the object can then be quantitatively retrieved by a proper combination of the measured images. Numerical experiments were carried out and the results confirmed the feasibility of the proposed method. It is expected that the proposed method will find widespread applications in biology, materials science and so on.

1. Introduction

The unique characteristics of X-rays are short wavelength and high penetration, and therefore X-ray microscopy is especially well suited to high-resolution tomographic imaging of several-micrometre-thick biological specimens (Kirz *et al.*, 1995). However, when imaging biological or other samples made of light elements with hard X-rays, the absorption contrast is always too weak (Henke *et al.*, 1993). Considering that the interaction of light with an object causes wavefront distortions, F. Zernike developed phase contrast microscopy (Zernike, 1942). This technique was then proven to be powerful for the observation of weak phase objects with the visible microscope. The phase contrast imaging method has also been successfully applied to X-ray microscopy (Schmahl *et al.*, 1995; Holzner *et al.*, 2010; Stampanoni *et al.*, 2010; Wang *et al.*, 2014). Following the development of high-quality Fresnel zone plates in the soft X-ray energy region, X-ray Zernike phase contrast imaging was first reported in 1995 (Schmahl *et al.*, 1995).

In the soft X-ray region, a zone-plate-based transmission X-ray microscope has achieved a spatial resolution of 12 nm (Chao *et al.*, 2009), and the advantage of using absorption information has already been successfully demonstrated in the 'water window' soft X-ray region (McDermott *et al.*, 2009; Larabell & Nugent, 2010; Hanssen *et al.*, 2011). However, the limited penetration of soft X-rays hinders widespread appli-

cations of soft X-ray microscopy. To overcome this limitation, the research activity of X-ray Zernike phase contrast microscopy has been shifted to the intermediate energy and hard X-ray region (Awaji *et al.*, 2002; Tkachuk *et al.*, 2007; Yin *et al.*, 2007; Liu *et al.*, 2011; Yuan *et al.*, 2012; Wang *et al.*, 2013; Vartiainen *et al.*, 2014*a*,*b*; Yang *et al.*, 2014). This trend is partly due to the fact that, within these energy regimes, and for biomedical samples, the real part of the complex refractive index, which describes the phase shift property, is always much larger than the imaginary part describing the absorption property. Moreover, the ratio between the real and imaginary part increases with the incident photon energy (Henke *et al.*, 1993). So it is obvious that the phase contrast is more conspicuous in the intermediate and hard X-ray region. As recently reported, in the intermediate X-ray range, a Zernike phase contrast microscope can provide good image contrast for biological samples (Wang *et al.*, 2013).

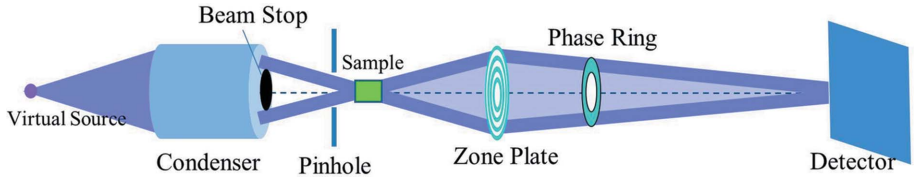

Figure 1
Schematic setup of X-ray Zernike phase contrast microscopy.

For an X-ray microscope operated in the Zernike phase contrast mode, the measured image intensity contains a mixture of absorption and phase information. As a consequence, the interpretation of the image and the quantitative tomographic reconstruction require a quantitative retrieval of the phase information from intensity measurements in X-ray Zernike phase contrast microscopy. Quantitative phase retrieval in a transmission X-ray microscope was reported for the first time by Yin *et al.* They put forward a combination of the transport of intensity equation (Teague, 1983) and the self-consistent wave propagation method (Allen *et al.*, 2004) to extract quantitative phase information of the sample (Yin *et al.*, 2007). But this method required a series of sample intensity images, where multiple exposures could induce serious radiation damage to biological samples. Working with a transmission X-ray microscope, Liu *et al.* (2011) introduced a new quantitative phase retrieval method, where a series of the sample's intensity images were measured by changing the energy of the incident X-rays. Several exposures were also required in this approach.

In this contribution, we propose an approach for quantitative phase retrieval in X-ray Zernike phase contrast microscopy, which takes advantage of the quantitative phase measurements in optical microscopy (Fiolka *et al.*, 2009; Gao *et al.*, 2011). The key point of this method is the use of two different phase rings. With the two phase rings put in the beam successively, two intensity measurements are recorded. By a proper combination of the two intensity images, we can retrieve quantitative phase information of the investigated sample. Numerical experiments are carried out, and the results confirm the validity of the proposed method.

2. Methods

A schematic diagram of X-ray Zernike phase contrast microscopy is shown in Fig. 1. Typically, a capillary reflective condenser produces hollow cone illumination, which is designed to nearly match the numerical aperture of the zone plate objective. Then, the light illuminating the sample is divided into a diffracted and an undiffracted part. The undiffracted light (*i.e.* direct light) passes through the phase ring, which is placed at the back focal plane of the zone plate objective, and then interferes with the diffracted light in the detector plane. Finally, the phase modulations of the sample are translated into intensity modulations recorded by the detector.

In the following, we derive the approach for quantitative phase retrieval in a transmission X-ray microscope operated in Zernike phase contrast mode. The interactions of X-rays with matter can be described by the complex refractive index: $n = 1 - \delta - i\beta$, where the real part δ represents the phase shift property and the imaginary part β the absorption of the material.

Consider a model object where a feature of interest is embedded in its homogeneous background. Assuming monochromatic plane wave illumination of unit amplitude, the complex amplitude A_f traveling through the particular feature is (Rudolph *et al.*, 1990; Wang *et al.*, 2013)

$$A_\mathrm{f} = \exp(-2\pi\beta_\mathrm{f}t/\lambda)\exp(i2\pi\delta_\mathrm{f}t/\lambda) \times \exp\left[-2\pi\beta_\mathrm{b}(D-t)/\lambda\right]\exp\left[i2\pi\delta_\mathrm{b}(D-t)/\lambda\right], \quad (1)$$

where λ is the X-ray wavelength, δ_f and β_f are the real and imaginary parts of the refractive index of the feature, respectively, δ_b and β_b are the real and imaginary parts of the refractive index of the background material, respectively, and D and t denote the thickness of the background and the feature, respectively. The complex amplitude A_b traveling through the homogeneous background is given by

$$A_\mathrm{b} = \exp(-2\pi\beta_\mathrm{b}t/\lambda)\exp(i2\pi\delta_\mathrm{b}t/\lambda) \times \exp\left[-2\pi\beta_\mathrm{b}(D-t)/\lambda\right]\exp\left[i2\pi\delta_\mathrm{b}(D-t)/\lambda\right]. \quad (2)$$

The insertion of the feature generates diffraction, and the amplitude of the diffracted wave can be approximated by $A_\mathrm{d} = A_\mathrm{f} - A_\mathrm{b}$.

In Zernike phase contrast mode, the wave A_b passes through the phase ring with a thickness t_p, the complex amplitude transmission of which is given by

$$T_\mathrm{p} = \exp\left(-2\pi\beta_\mathrm{p}t_\mathrm{p}/\lambda\right)\exp\left(i2\pi\delta_\mathrm{p}t_\mathrm{p}/\lambda\right), \quad (3)$$

where δ_p and β_p represent the real and imaginary parts of the refractive index of the phase ring material, respectively. To obtain Zernike phase contrast, the thickness of the phase ring is designed to introduce a phase shift of the undiffracted light

by $\pi/2$ (positive phase contrast) or $3\pi/2$ (negative phase contrast). Herein, we assume that the modulation transfer function of the detector is 100% for all spatial frequencies. Then, the amplitude of the feature image can be written as

$$A = A_b T_p + A_d \tag{4}$$

and the corresponding intensity is given by

$$I = A^* A. \tag{5}$$

In the absence of a feature, the surroundings' intensity is given by

$$I_b = A_b^* T_p^* A_b T_p. \tag{6}$$

So the normalized sample's intensity image is given by

$$I' = I/I_b. \tag{7}$$

In the proposed phase retrieval method, we use two different phase rings. One is for the positive phase contrast and the other for the negative phase contrast. In the positive phase contrast mode the thickness of the phase ring satisfies $2\pi\delta_p t_{p1}/\lambda = \pi/2$, and one has $T_{p1} = i\exp(-2\pi\beta_p t_{p1}/\lambda)$. Then the amplitude of the feature image is given by

$$\begin{aligned} A_1 &= A_b T_{p1} + A_d \\ &= \exp\left[-2\pi\beta_b(D-t)/\lambda\right]\exp\left[i2\pi\delta_b(D-t)/\lambda\right] \\ &\quad\times\Big\{i\left[a_1\exp(-2\pi\beta_b t/\lambda)\exp(i2\pi\delta_b t/\lambda)\right] \\ &\quad+\exp(-2\pi\beta_f t/\lambda)\exp(i2\pi\delta_f t/\lambda) \\ &\quad-\exp(-2\pi\beta_b t/\lambda)\exp(i2\pi\delta_b t/\lambda)\Big\}, \end{aligned} \tag{8}$$

with $a_1 = \exp(-2\pi\beta_p t_{p1}/\lambda)$. The image intensities with and without the feature are given by

$$\begin{aligned} I_1 = A_1^* A_1 &= \exp(-4\pi\beta_b D/\lambda)\Big\{a_1^2 + 1 + \exp\left[4\pi(\beta_b-\beta_f)t/\lambda\right] \\ &\quad+2(a_1\sin\varphi-\cos\varphi)\exp\left[2\pi(\beta_b-\beta_f)t/\lambda\right]\Big\}, \end{aligned} \tag{9}$$

$$\begin{aligned} I_{b1} &= A_b^* T_{p1}^* A_b T_{p1} \\ &= \exp\left(-4\pi\beta_p t_{p1}/\lambda\right)\exp(-4\pi\beta_b D/\lambda) \\ &= a_1^2\exp(-4\pi\beta_b D/\lambda), \end{aligned} \tag{10}$$

respectively, where $\varphi = 2\pi(\delta_f-\delta_b)t/\lambda$. We obtain the normalized intensity image,

$$\begin{aligned} I_1' = \frac{I_1}{I_{b1}} &= \frac{1}{a_1^2}\Big\{a_1^2 + 1 + \exp\left[4\pi(\beta_b-\beta_f)t/\lambda\right] \\ &\quad+2(a_1\sin\varphi-\cos\varphi)\exp\left[2\pi(\beta_b-\beta_f)t/\lambda\right]\Big\}. \end{aligned} \tag{11}$$

In transmission X-ray microscopy, the typical feature size is of the order of tens of nanometres. Therefore we can reasonably apply the first-order Taylor expansion to (11),

$$\begin{aligned} \exp\left[4\pi(\beta_b-\beta_f)t/\lambda\right] &\approx 1 + 4\pi(\beta_b-\beta_f)t/\lambda, \\ \exp\left[2\pi(\beta_b-\beta_f)t/\lambda\right] &\approx 1 + 2\pi(\beta_b-\beta_f)t/\lambda. \end{aligned} \tag{12}$$

Under the above approximation, the normalized intensity image has the following expression, and a detailed derivation from equations (11) to (13) can be found in Appendix *A*,

$$I_1' \approx \left\{a_1^2 + 2(1 + a_1\sin\varphi - \cos\varphi)\left[1 + 2\pi(\beta_b-\beta_f)t/\lambda\right]\right\}/a_1^2. \tag{13}$$

In the negative phase contrast mode, a second phase ring is utilized. The thickness is chosen to introduce a $3\pi/2$ phase shift onto the undiffracted beam. Following a procedure similar to that used for the positive phase contrast mode, we obtain the corresponding normalized image intensity,

$$I_2' \approx \left\{a_2^2 + 2(1 - a_2\sin\varphi - \cos\varphi)\left[1 + 2\pi(\beta_b-\beta_f)t/\lambda\right]\right\}/a_2^2, \tag{14}$$

with $a_2 = \exp(-2\pi\beta_p t_{p2}/\lambda)$. By a proper combination of equations (13) and (14), we can retrieve the phase shift of the feature given by

$$\sin\varphi/(1-\cos\varphi) = B, \tag{15}$$

$$\varphi = \arcsin\left[2B/\left(B^2+1\right)\right], \tag{16}$$

where $B = (a_1^2 I_1' - a_2^2 I_2' - a_1^2 + a_2^2)/\{a_1 a_2[a_1 I_1' + a_2 I_2' - (a_1 + a_2)]\}$.

A detailed derivation of equations (15) and (16) can be found in Appendix *B*. Equation (16) represents the main result of this contribution, *i.e.* the phase retrieval method. By use of two intensity measurements with two different phase rings, we can retrieve the phase shift of the sample quantitatively. Note that in the derivation of (16) we have used the linear approximation given in equation (12). When the linear approximation does not hold well, the retrieval result by use of (16) will deviate from the theoretical true values. To validate the proposed method, we numerically simulated an X-ray Zernike phase contrast microscope and performed phase retrieval using measured image intensities.

3. Results and discussion

Numerical experiments are performed to demonstrate the feasibility of the proposed method. We simulated an X-ray Zernike phase contrast microscope with a photon energy of 2.5 keV (Wang *et al.*, 2013). A Fresnel zone plate (400 nm-thick Au, 30 nm outmost zone width) was used as the objective to reach a spatial resolution better than 30 nm. The microscope used two phase rings made of nickel; one was $\pi/2$-phase shifting and the other was $3\pi/2$-phase shifting. In our simulation, Poisson-distributed shot noise is considered in the measured images.

Two test samples are constructed for both quantitative measurement and evaluation. The refractive index of the test samples are found from the *Index of Refraction* data (http://henke.lbl.gov/optical_constants/getdb2.html). The first test sample is a plastic zone plate made of polymethyl methacrylate (PMMA) on silicon nitride (Yin *et al.*, 2007). This sample acts as a representative of a weakly absorbing object. The thicknesses were set to 1000 nm, 800 nm, 600 nm, 400 nm, 200 nm and 200 nm from the inner to the outer rings, to test the feasibility of the proposed method in the case of distinct phase shifts.

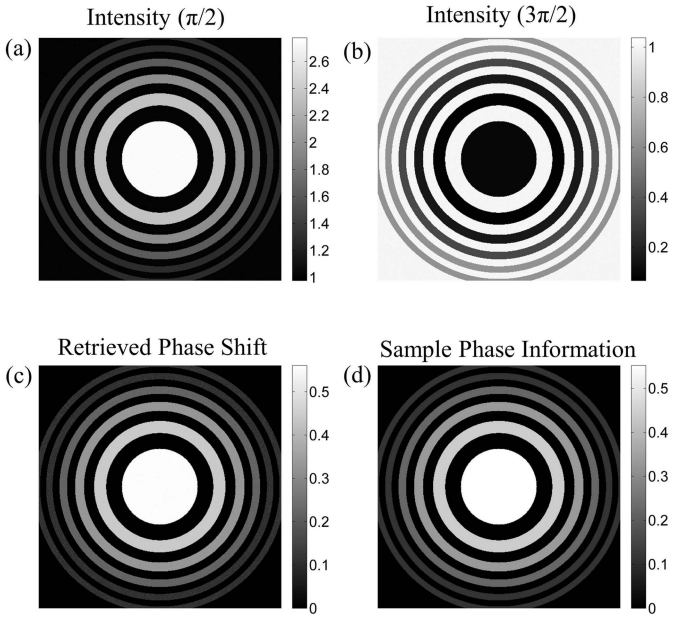

Figure 2
(*a*), (*b*) Intensity images of the sample with a $\pi/2$ phase ring and a $3\pi/2$ phase ring, respectively. (*c*), (*d*) Retrieved phase shift and the true phase shift of the sample, respectively.

The results of the first sample are shown in Fig. 2. Figs. 2(*a*) and 2(*b*) present the simulated intensity images for a $\pi/2$ phase ring and a $3\pi/2$ phase ring, respectively. In these two images, Poisson-distributed shot noise is added. As expected, contrast reversal appears owing to the different phase shifts. With these two images as input, we retrieved the phase shift of the sample by use of equations (15) and (16), and the result is shown in Fig. 2(*c*). For comparison, Fig. 2(*d*) displays the true phase shift of the sample. As can be seen, Figs. 2(*c*) and 2(*d*) match well qualitatively. Furthermore, a line profile comparison is performed. As shown in Fig. 3, a quantitative agreement is achieved. It is noted that a phase shift as large as 0.55 rad can be retrieved precisely. The small mismatch in the region of the outer ring can be attributed to the added shot noise. The results shown in Figs. 2 and 3 confirm the feasibility of the proposed method in the case of weak absorption objects.

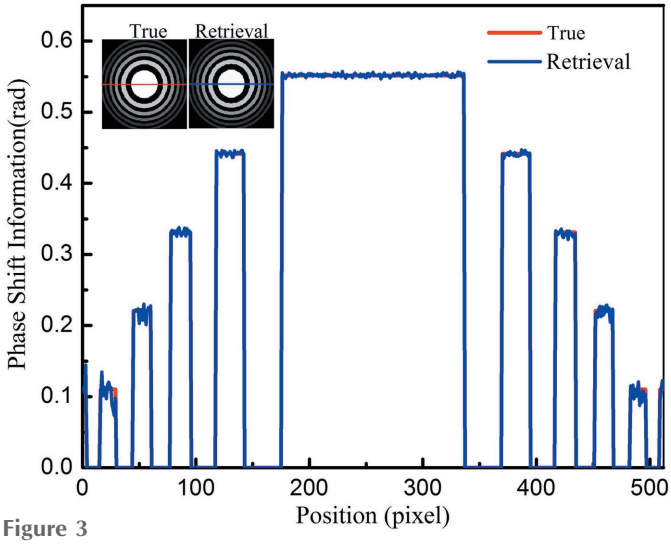

Figure 3
Line profile comparison between the true and retrieved phase shift of the sample.

The second test sample is a Siemens star-like sample made of copper, which is surrounded by water with a thickness of 5 μm. This sample represents a high-absorption feature in a cellular environment. The thickness of the copper ranged from 30 nm to 105 nm in steps of 5 nm arranged anticlockwise in a fan of angle $\pi/16$.

The results of the second sample are shown in Fig. 4. The simulated intensity images are shown in Figs. 4(*a*) and 4(*b*) for $\pi/2$ and $3\pi/2$ phase rings, respectively. Again, one can see the reversed contrast in these two images. By use of equation (16), the sample phase is retrieved, and the result is presented in Fig. 4(*c*). For comparison, Fig. 4(*d*) shows the true phase information of the sample. Note that Figs. 4(*c*) and 4(*d*) are visually in good agreement. Furthermore, Fig. 5 shows the line profile for a quantitative comparison. As can be seen, the retrieval result is seriously contaminated by the added shot noise when the thickness is less than 35 nm. With a thickness range from 40 nm to 80 nm, the retrieved phase shift is an excellent match with the true value. This again confirms the effectiveness of the proposed method. With further increasing thickness, the phase shift is overestimated by use of equation (16), and the error becomes greater. This can be explained by the violation of the validity of the first-order approximation used in equation (12). With a 50 nm thickness, the intensity transmission is 0.9492, which can be well approximated by 0.9478. However, when the thickness is increased to 100 nm, the transmission decreases to 0.9009. The linear approximation does not hold well, which then results in an error in the

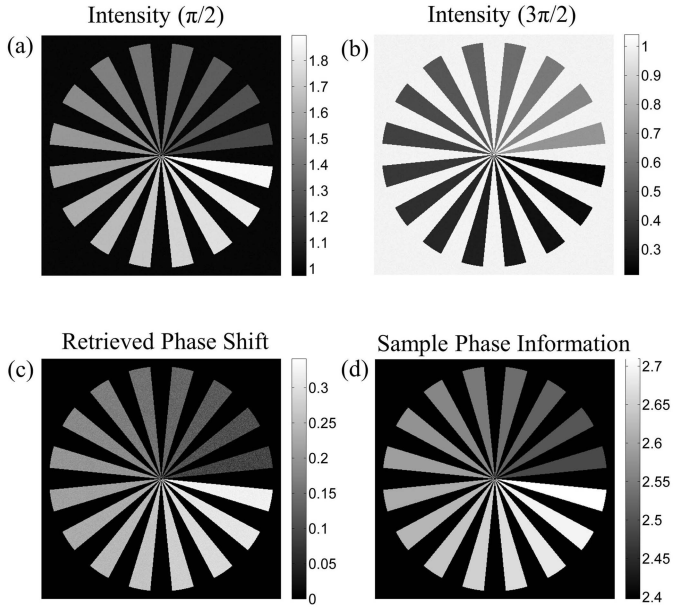

Figure 4
(*a*), (*b*) Intensity images of a copper Siemens-like star sample with a $\pi/2$ and a $3\pi/2$ phase ring, respectively. (*c*), (*d*) Retrieved phase shift and the true phase information of the sample, respectively. The thickness of the copper features increases in an anticlockwise direction from 30 nm at the 3 o'clock position to 105 nm in 5 nm steps.

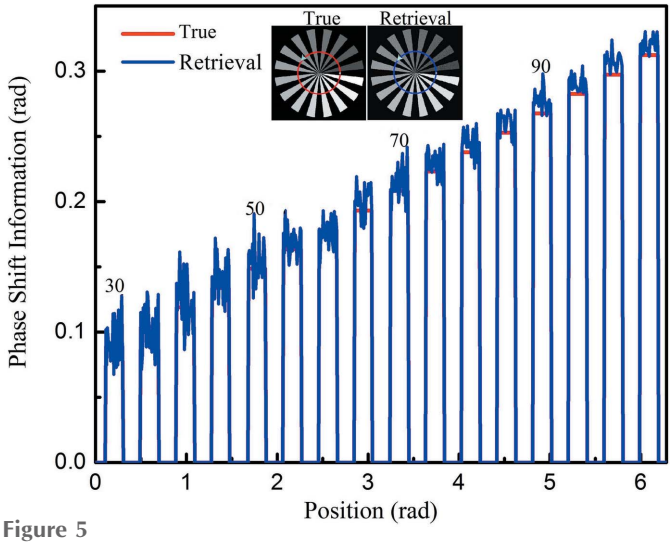

Figure 5
Profile comparison between the true and retrieved phase shift of the second sample. The numbers on the figure (30, 50, 70 and 90) indicate the thickness of the respective features in the sample in nanometers.

retrieved phase shift. In experiments, one can estimate the absorption of the investigated object before imaging, and then use this knowledge to modify the retrieved phase shift to be correct. Furthermore, we would like to mention that in the case of a 10% X-ray attenuation, the resulting absorption contrast is already sufficient for imaging purposes.

4. Conclusion

In conclusion, we have presented a quantitative phase retrieval method in X-ray Zernike phase contrast microscopy. With the use of two distinct phase rings, two sample images are measured successively. The phase shift information can then be quantitatively retrieved by properly dealing with the two intensity measurements. Numerical experiments are performed for the cases of both weak and strong absorption objects. For these weakly absorbing objects, a good agreement is achieved between the retrieval results and theoretical true values, thus confirming the feasibility of the proposed method. However, for those objects of strong absorption, some discrepancies are observed between the retrieved results and the true values. This can be attributed to the violation of the used approximation, and may be corrected by use of prior knowledge. With the further development of X-ray optics and technologies, the proposed method may find widespread implementations at synchrotron radiation facilities.

APPENDIX *A*
Detailed mathematic derivation from equation (11) to equation (13)

Combine equation (11) with equation (12), and equation (13) is calculated by

$$\begin{aligned} I_1' &\approx \frac{1}{a_1^2}\Big\{a_1^2+1+\big[1+4\pi(\beta_b-\beta_f)t/\lambda\big] \\ &\quad +2(a_1\sin\varphi-\cos\varphi)\big[1+2\pi(\beta_b-\beta_f)t/\lambda\big]\Big\} \\ &= \frac{1}{a_1^2}\Big\{a_1^2+2\big[1+2\pi(\beta_b-\beta_f)t/\lambda\big] \\ &\quad +2(a_1\sin\varphi-\cos\varphi)\big[1+2\pi(\beta_b-\beta_f)t/\lambda\big]\Big\} \\ &= \frac{1}{a_1^2}\big\{a_1^2+2(1+a_1\sin\varphi-\cos\varphi)\big[1+2\pi(\beta_b-\beta_f)t/\lambda\big]\big\}. \end{aligned} \tag{17}$$

Similarly, equation (14) is calculated by

$$\begin{aligned} I_2' = \frac{I_2}{I_{b2}} &= \frac{1}{a_2^2}\Big\{a_2^2+1+\exp\big[4\pi(\beta_b-\beta_f)t/\lambda\big] \\ &\quad +2(-a_2\sin\varphi-\cos\varphi)\exp\big[2\pi(\beta_b-\beta_f)t/\lambda\big]\Big\} \\ &\approx \frac{1}{a_2^2}\Big\{a_2^2+1+\big[1+4\pi(\beta_b-\beta_f)t/\lambda\big] \\ &\quad +2(-a_2\sin\varphi-\cos\varphi)\big[1+2\pi(\beta_b-\beta_f)t/\lambda\big]\Big\} \\ &= \frac{1}{a_2^2}\Big\{a_2^2+2\big[1+2\pi(\beta_b-\beta_f)t/\lambda\big] \\ &\quad +2(-a_2\sin\varphi-\cos\varphi)\big[1+2\pi(\beta_b-\beta_f)t/\lambda\big]\Big\} \\ &= \frac{1}{a_2^2}\Big\{a_2^2+2(1-a_2\sin\varphi-\cos\varphi) \\ &\quad \times\big[1+2\pi(\beta_b-\beta_f)t/\lambda\big]\Big\}. \end{aligned} \tag{18}$$

So the normalized intensity image with a $\pi/2$ phase ring and $3\pi/2$ phase ring can be given by equations (13) and (14), respectively.

APPENDIX *B*
Detailed mathematic derivation of equations (15) and (16)

According to the formula $a_1^2[(17)]-a_2^2[(18)]$, we obtain the expression

$$a_1^2I_1'-a_2^2I_2'=a_1^2-a_2^2+2(a_1+a_2)\big[1+2\pi(\beta_b-\beta_f)t/\lambda\big]\sin\varphi, \tag{19}$$

and (19) is equivalent to

$$\big[1+2\pi(\beta_b-\beta_f)t/\lambda\big]\sin\varphi=\frac{a_1^2I_1'-a_2^2I_2'-a_1^2+a_2^2}{2(a_1+a_2)}. \tag{20}$$

According to the formula: $a_1^2a_2[(17)]+a_1a_2^2[(18)]$, we obtain the following expression,

$$
\begin{aligned}
a_1^2 a_2 I_1' + a_1 a_2^2 I_2' &= \left\{a_1^2 a_2 + 2a_2(1 + a_1 \sin\varphi - \cos\varphi)\right. \\
&\quad \left.\times \left[1 + 2\pi(\beta_b - \beta_f)t/\lambda\right]\right\} \\
&\quad + \left\{a_1 a_2^2 + 2a_1(1 - a_2 \sin\varphi - \cos\varphi)\right. \\
&\quad \left.\times \left[1 + 2\pi(\beta_b - \beta_f)t/\lambda\right]\right\} \\
&= a_1^2 a_2 + a_1 a_2^2 + 2(a_1 + a_2)(1 - \cos\varphi) \\
&\quad \times \left[1 + 2\pi(\beta_b - \beta_f)t/\lambda\right], \qquad (21)
\end{aligned}
$$

and equation (21) is equivalent to

$$
\begin{aligned}
&\left[1 + 2\pi(\beta_b - \beta_f)t/\lambda\right](1 - \cos\varphi) \\
&\qquad = \frac{a_1^2 a_2 I_1' + a_1 a_2^2 I_2' - \left(a_1^2 a_2 + a_1 a_2^2\right)}{2(a_1 + a_2)} \\
&\qquad = \frac{a_1 a_2\left[a_1 I_1' + a_2 I_2' - (a_1 + a)\right]}{2(a_1 + a_2)}. \qquad (22)
\end{aligned}
$$

By calculating the ratio [(20)]/[(22)], equation (15) is given by

$$
\frac{\sin\varphi}{(1 - \cos\varphi)} = \frac{a_1^2 I_1' - a_2^2 I_2' - a_1^2 + a_2^2}{a_1 a_2\left[a_1 I_1' + a_2 I_2' - (a_1 + a)\right]}, \qquad (23)
$$

and equation (23) is equivalent to

$$
\frac{\sin\varphi}{(1 - \cos\varphi)} = B, \qquad (24)
$$

where $B = a_1^2 I_1' - a_2^2 I_2' - a_1^2 + a_2^2/\{a_1 a_2[a_1 I_1' + a_2 I_2' - (a_1 + a)]\}$, and equation (24) is equal to equation (15).

In the following, equation (24) is replaced by

$$
\cos\varphi = \frac{B - \sin\varphi}{B}. \qquad (25)
$$

With the use of the relationship in the trigonometrically function $\sin^2\varphi + \cos^2\varphi = 1$, one obtains

$$
\begin{aligned}
&\sin^2\varphi + \cos^2\varphi = \sin^2\varphi + \left(\frac{B - \sin\varphi}{B}\right)^2 = 1 \\
&\Rightarrow \frac{B^2 \sin^2\varphi + B^2 - 2B\sin\varphi + \sin^2\varphi}{B^2} = 1 \qquad (26) \\
&\Rightarrow \sin\varphi = \frac{2B}{B^2 + 1} \\
&\Rightarrow \varphi = \arcsin\left[2B/\left(B^2 + 1\right)\right],
\end{aligned}
$$

and equation (26) is equal to equation (16).

Acknowledgements

This work was supported by the States Key Project for Fundamental Research (2012CB825801), the National Natural Science Foundation of China (11205157, 11475170), and Anhui Provincial Natural Science Foundation (1508085 MA20).

References

Allen, L. J., McBride, W., O'Leary, N. L. & Oxley, M. P. (2004). *Ultramicroscopy*, **100**, 91–104.
Awaji, M., Suzuki, Y., Takeuchi, A., Takano, H., Kamijo, N., Tamura, S. & Yasumoto, M. (2002). *J. Synchrotron Rad.* **9**, 125–127.
Chao, W., Kim, J., Rekawa, S., Fischer, P. & Anderson, E. H. (2009). *Opt. Express*, **17**, 17669–17677.
Fiolka, R., Wicker, K., Heintzmann, R. & Stemmer, A. (2009). *Opt. Express*, **17**, 12407–12417.
Gao, P., Yao, B., Harder, I., Lindlein, N. & Torcal-Milla, F. J. (2011). *Opt. Lett.* **36**, 4305–4307.
Hanssen, E., Knoechel, C., Klonis, N., Abu-Bakar, N., Deed, S., LeGros, M., Larabell, C. & Tilley, L. (2011). *J. Struct. Biol.* **173**, 161–168.
Henke, B. L., Gullikson, E. M. & Davis, J. C. (1993). *At. Data Nucl. Data Tables*, **54**, 181–342.
Holzner, C., Feser, M., Vogt, S., Hornberger, B., Baines, S. B. & Jacobsen, C. (2010). *Nat. Phys.* **6**, 883–887.
Kirz, J., Jacobsen, C. & Howells, M. (1995). *Q. Rev. Biophys.* **28**, 33–130.
Larabell, C. A. & Nugent, K. A. (2010). *Curr. Opin. Struct. Biol.* **20**, 623–631.
Liu, Y., Andrews, J. C., Wang, J., Meirer, F., Zhu, P., Wu, Z. & Pianetta, P. (2011). *Opt. Express*, **19**, 540–545.
McDermott, G., Le Gros, M. A., Knoechel, C. G., Uchida, M. & Larabell, C. A. (2009). *Trends Cell Biol.* **19**, 587–595.
Rudolph, D., Schmahl, G. & Niemann, B. (1990). *Amplitude and Phase Contrast in X-ray Microscopy*. New York: Plenum.
Schmahl, G., Rudolph, D., Guttmann, P., Schneider, G., Thieme, J. & Niemann, B. (1995). *Rev. Sci. Instrum.* **66**, 1282–1286.
Stampanoni, M., Mokso, R., Marone, F., Vila-Comamala, J., Gorelick, S., Trtik, P., Jefimovs, K. & David, C. (2010). *Phys. Rev. B*, **81**, 140105.
Teague, M. R. (1983). *J. Opt. Soc. Am.* **73**, 1434–1441.
Tkachuk, A., Duewer, F., Cui, H., Feser, M., Wang, S. & Yun, W. (2007). *Z. Kristallogr.* **222**, 650–655.
Vartiainen, I., Mokso, R., Stampanoni, M. & David, C. (2014*b*). *Opt. Lett.* **39**, 1601–1604.
Vartiainen, I., Warmer, M., Goeries, D., Herker, E., Reimer, R., David, C. & Meents, A. (2014*a*). *J. Synchrotron Rad.* **21**, 790–794.
Wang, D., Li, N., Wang, Z., Gao, K., Zhang, Y., Luo, Y., Wang, S., Bao, Y., Shao, Q. & Wu, Z. (2014). *J. Synchrotron Rad.* **21**, 1175–1179.
Wang, Z., Gao, K., Chen, J., Hong, Y., Ge, X., Wang, D., Pan, Z., Zhu, P., Yun, W., Jacobsen, C. & Wu, Z. (2013). *Biotechnol. Adv.* **31**, 387–392.
Yang, Y., Heine, R., Cheng, Y., Wang, C. C., Song, Y. F. & Baumbach, T. (2014). *Appl. Phys. Lett.* **105**, 094101.
Yin, G. C., Chen, F. R., Hwu, Y., Shieh, H. D. & Liang, K. S. (2007). *Appl. Phys. Lett.* **90**, 181118.
Yuan, Q., Zhang, K., Hong, Y., Huang, W., Gao, K., Wang, Z., Zhu, P., Gelb, J., Tkachuk, A., Hornberger, B., Feser, M., Yun, W. & Wu, Z. (2012). *J. Synchrotron Rad.* **19**, 1021–1028.
Zernike, F. (1942). *Physica*, **9**, 974–986.